Flow characterization of various singularities in a real-scale ventilation network with rectangular ducts

Jeanne Malet, Marko Radosavljevic, Modou Mbaye, Delphine Costa, Johann Wiese, Evelyne Géhin

FLOW CHARACTERIZATION OF VARIOUS SINGULARITIES IN A REAL-SCALE VENTILATION NETWORK WITH RECTANGULAR DUCTS

J. MALET[1*], M. RADOSAVLJEVIC[1], M. MBAYE[1], D. COSTA[1,2], J. WIESE[1], E. GEHIN[2]

[1]Institut de Radioprotection et de Sûreté Nucléaire (IRSN), PSN-RES, SCA, LEMAC, Gif-sur-Yvette, 91192, France

jeanne.malet@irsn.fr ; marko.radosavljevic@irsn.fr; modou.mbaye@irsn.fr; delphine.costa-upec@irsn.fr; johann.wiese@irsn.fr; gehin@u-pec.fr

[2] Univ Paris Est Creteil, CERTES, F-94000 Creteil, France

gehin@u-pec.fr

*corresponding author

ABSTRACT

Flow characterization in ventilation ducts is important for adequate modelling of contamination transfer in various contexts. Turbulent flow through straight tubes with circular cross-section has, generally, been widely studied, but HVAC networks are quite unlike such ideal cases. Industrial ducts are of large scale, their sections can be rectangular, and include many singularities, such as bends, T-junctions, reducers, valves, etc., which can modify the flow pattern.

The objective of this paper is to study the effect of various singularities on flow in real-scale rectangular ventilation ducts. Flow measurements are performed in a 60 m-long industrial ventilation network (600 x

400 mm²) which includes over ten vertical and horizontal bends, one T-junction with a ventilation damper located in the secondary branch, and one section reducer. Horizontal velocity profiles are measured using hot wire anemometry. The effects on the flow of a deflector inserted in a bend, of a damper leak, and of a damper opening are presented using experimental measurement and numerical simulation using ANSYS/Fluent with second-order turbulence models (RSM) validated on a DNS case. These tests form an extensive database for flow measurements at industrial scale, useful for CFD validation, a necessary step before simulating gaseous and particulate flow in ventilation ducts.

KEYWORDS

DUCT, VENTILATION, BEND, DEFLECTOR, T-JUNCTION, DAMPER

1. INTRODUCTION

Flow characterization and modeling in ducts is important for various applications. The earliest application is probably the quality of the main flow-rate measurement which is dependent on the location of the velocity measurement points in the duct section. Recommendations exist for performing such measurements (international standards ISO 3966, ISO 7145, DIN EN 12599 [1], Dinardo *et al.* 2016 [2]), generally by taking the measurement in a zone where turbulent flow is assumed established. However, in real-scale applications, flow establishment is difficult to obtain, raising many questions regarding the representativeness of flow-rate measurements in duct flows. The same problem exists for aerosol sampling representativeness, which is still an open field of research.

The second main field of interest for duct flow studies are HVAC systems which are, obviously, the most direct application, whether regarding heat losses for energy consumption evaluation or noise reduction for residential/industrial comfort. HVAC design in the early stages of the building design process also implies a need for adequate modeling of HVAC systems. Indoor air quality, and more recently, with the Covid19 pandemic, SARS-CoV-2 propagation through typical offices and ventilation systems, are other kinds of applications in which duct flow is the basis of aerosol and/or droplet transport and dispersion.

Flow in ventilation ducts is also of primary importance for aerosol transfer in many other industrial applications and/or processes. In nuclear buildings and plants, transfer within ventilation ducts can lead to local accumulation of radioactive material by particle deposition in duct singularities, entailing a radiological risk during maintenance operations on or near these singularities. These deposited particles can also be resuspended and transferred through the same ventilation network, depending on many parameters, among which the turbulent flow characteristics are of primary importance. Quantifying the deposit makes it possible to better assess the impact of the aerosol on the filters by clogging as well. The

modelling of aerosol deposition is a subject of many past studies (Sippola and Nazaroff, 2004 [3], Wu and Zhao, 2007 [4], Ben Othman *et al.* 2011 [5], Jiang *et al.* 2011 [6], Lu and Wang, 2019 [7]) and remains a challenging task enhanced by the fact that deposition measurement is not a standard measurement technique (Costa *et al.* 2022 [8]). This accumulation and resuspension effect is also a concern for biological aerosols in ventilation ducts in food factories, making agribusiness another application for duct flow studies. Other industrial fields involving dust particulate matter transported through ventilation ducts also need adequate description of flow modeling, especially in singularities such as elbows, for risk assessment on sand erosion in the duct in local zones where sand particles mainly impact (Sommerfeld and Lain, 2018 [9]).

In coal-fired power plants which continuously supply pulverized coal to furnaces, coal particles are transported through ducts consisting in numerous bends and straight sections; these changes in flow direction, combined with the large size of the coal particles (10 to 1000 μm) lead to non-uniform particle concentrations, making it difficult to control the fuel droplet supply to individual burners.

Industrial accidents and fires are another type of situation for which good modeling of turbulent duct flow is needed, especially for soot particle transport under extreme temperature conditions which necessarily creates other flow patterns in the duct as well as in the singularities of the ventilation network.

All these applications generally lead to engineering models developed to simulate the performance or losses of a ventilation duct according to the specific case. Afram and Janabi-Sharifi (2014) [10] present a review of modeling methods for HVAC systems for numerous applications. The French Institute for Radiological Protection and Nuclear Safety (IRSN) develops the SYLVIA code (Chojnacki *et al.*, 2019 [11]) enabling characterization of pressure losses and aerosol (radioactive or soot) deposition in ventilation ducts under normal and accident conditions (fire propagation). This type of engineering

modeling requires validation of the various assumptions, hypotheses and simplifications of the phenomena. Validation is obtained through experiments which do not always allow exhaustive characterization of the flow inside the ducts, either because of difficult access to measurement zones, or because of the use of very local (point) measurements that do not allow multi-dimensional validation. Computational Fluid Dynamics (CFD) can then be a complementary tool for validating the engineering codes, once they themselves have been validated using experimental data. Depending on the application, different types of measurement may be performed for CFD validation types: pressure loss, aerosol deposition, noise reduction, temperature measurements. All of these are sensitive to one main variable: flow velocities and the associated turbulence parameters. In other words, simulation of one of these parameters requires adequate simulation of the flow velocity to avoid errors relating to the simulated phenomena.

Consequently, velocity and turbulence measurements in ventilation ducts are of prime importance and are thus the focus of numerous studies, as will briefly be presented in the State-of-the-Art section below. However, few such measurements are performed on real-scale ventilation networks comprising several rectangular straight lengths, horizontal and vertical bends of various shapes, T-junctions, reducers, circular-to-rectangular connections, etc.

In this paper, the work is based on a large-scale experimental test facility involving different straight-length ducts (shorter, medium, long), different types of bend (horizontal, vertical, U-shape, S-shape, with/without internal deflector), a T-junction, a symmetrical reducer and a ventilation damper. Part of this facility is designed especially devoted for the study of so-called “typical industrial systems”, such as internal deflectors often installed in industrial bends, dampers, fire dampers, flexible sleeves, etc. Implementation of Pitot tube, hot wire anemometry, and PIV are available at various points in the facility.

The objective of this paper aims to contribute to flow characterization in large-scale industrial rectangular ducts by performing experiments and associated CFD simulations. The objectives of the measurements performed using such a large-scale facility are manifold:

- To characterize the flow in straight ducts at several points downstream of a singularity.
- To study the flow upstream and downstream of a singularity, such as a bend, a T-junction, and a reducer.
- To study the impact of so-called "typical industrial systems" on flow measurements, such as a bend deflector, a damper leak, or a standard ventilation damper in various positions.

This paper starts with a presentation of the state of the art regarding past experimental measurements of velocity performed on ventilation ducts. In the second part, presentation of the experimental test bench and the numerical code with its associated preliminary verifications and validations will be given. Results will then be presented, first focusing on a standard geometrical configuration of a ventilation network (straight ducts, bend, T-junction and reducer). The second part of the discussion looks at typical industrial systems (bend deflector, residual leak from a flow damper and a standard ventilation damper).

2. STATE- OF THE -ART

Many studies exist on flow measurements in ducts but there are not many on large-scale rectangular ducts. Indeed, such studies generally focus on one or two components (one straight duct, one bend, one convergent section). Most of these are symmetrical (either circular or square cross-section) and studies are generally performed at small scale (few centimeters). For rectangular sections, the focus is generally on large aspect ratios (Hinze, 1973 [12], Rokni *et al.* 1998 [13]).

Table I presents several experimental studies involving detailed flow characterization performed on circular ducts of sizes generally lower than 20 cm diameter. A longitudinal velocity profile in a straight

duct is measured by Geropp and Odenthal (2002) [14] in order to compare the results to a velocity law. Sudo *et al.* (1998) [15] and Kalpakli and Orlu (2013) [16] performed measurements of velocity profiles inside a bend, at various locations, with the objective of observing secondary flows by measuring transverse components. Circular U-bend studies are presented in Azzola *et al.* (1986) [17] and Sudo *et al.* (2000) [18] where longitudinal measurements are performed. Other studies focus on more complex bend singularities, such as Caré *et al.* (2014) [19] who study co-planar and non-co-planar bends, and Sleiti *et al.* (2017) [20] who work on close-coupled bends. A wide range of measurement techniques is used in these studies, Pitot tube, hot wires, laser Doppler velocimetry, and Particle Image Velocimetry (PIV).

Table I. Experimental studies on circular ducts involving detailed flow measurements

Authors	Duct shape	Duct size (D_h R_c, L)	Exp. method	Reynolds	Location of measurements
Enayet *et al.* (1982) [21]	SD, L = 0.48 m, 90-bend	D_h = 4.8 cm R_c = 3.4 cm	LDA	4.3 10^4	U Profiles at 45° and 90° of a CB
Azzola *et al.* (1986) [17]	U-bend	*AR*=6.75	LDA	5.74. 10^4 11. 10^5	over z, between 90° to z/D = 5
Sudo *et al.* (1998) [15]	90-bend, L_u=10 m, L_d= 4.2 m	D_h=10.4 cm R_c=20.8 cm	HW SP on walls	6.10^4	z/d=-1 → z/d=5
Sudo *et al.* (2000) [18]	U-bend	D_h=10.4 cm R_c=20.8 cm	HW	6.10^4	21 points inside the U
Geropp and Odenthal (2002) [14]	SD, L = 6.08 m	D_h=7.6 cm	LDA, SP	1.49 10^5 1.86 10^5	Longitudinal profile
Kalpakli and Orlu (2013) [16]	bend	D_h=6.03cm R_c=1.58 D_h	Stereo PIV HW	1.4 10^4 to 3.4 10^4	Three profiles and transverse fields
Caré *et al.* (2014) [19]	2 co-planar and 2 non-coplanar bends	D_h=20 cm	PT	2 10^5	10-point profiles at z/d = 1, 4, 10 and 45
Sleiti *et al.* (2017) [20]	Close-coupled bends (Z and U-shape)	D_h=30.5 cm R_c=1.5 D_h	PT - Five-hole U-probe	3.3 10^5 to 3.6 10^5	

Key – AR: Aspect Ratio, PIV: Particle Image Velocimetry, LDA: Laser Doppler Anemometry, HW: Hot Wire, PT: Pitot Tube, SP: Static Pressure measurement, L_u: upstream Length, L_d: downstream Length, D_h: hydraulic Diameter, R_c: curvature Radius, z: longitudinal direction, r: radial direction

Experimental studies in square ducts and rectangular ducts (Table II and Table III) are mainly performed with hot wire and LDA measurements. It can also be noted that measurements of the longitudinal flow

components are available in the open literature, but there are only a few experiments on the experimental characterization of secondary flows. Demuren and Rodi (1984) [22] synthetize most of the very first experimental studies on secondary flows in non-circular ducts. Launder *et al.,* (1972) [23], Gessner *et al.*, (1979) [24] and Kliafas and Holt (1987) [25] and others listed in Table II present experimental data, generally for straight ducts but also sometimes correlated with bend flow studies. Further studies on rectangular ducts are detailed in Table III, such as Melling and Whitelaw, (1976) [26], Fujita *et al.*, (1989) [27], Knight *et al.*, (1985) [28], Maeda *et al.*, (2005) [29]. Regarding the configurations of the rectangular channels, studies are rather limited in number over the last forty years: experimental studies either focus on straight length or on one bend: none of the experiments consider several singularities in the same facility. Furthermore, these experimental studies are performed on academic scales, ranging between a few centimeters up to 15-25 cm.

In addition to real-scale experimental studies, more DNS calculations are being performed, especially on secondary flows in various types of ducts; such results provide a wide range of valuable information (Huser *et al.*, 1993 [30], Gavrilakis, 1992 [31] , Zhang *et al.* 2015 [32]) on small-scale fictitious ducts.

Table II. Experimental studies on square ducts involving detailed flow measurements

Authors	Shape	Section size	Tech.	Reynolds	Comment
Brundrett and Baines (1964) [33]	SD, L = 21 m	D_h = 7.5 cm	HW	8.3 10^4	Data table of mean velocities and turbulent correlations
Gessner and Jones (1965) [24]	SD, L = 2.9 m	D_h = 7.2 cm	PT, HW	7.5 10^4 to 3 10^5	U_{transv} and Reynolds stress profiles in an octant
Launder and Ying (1972) [23]	SD, L = 5.7 m	D_h = 10 cm	HW	2.1 10^4 6.9 10^4	U_{long} and U_{transv} profiles for rough and smooth duct
Gessner *et al.* (1979) [38]	SD, L = 22 m	D_h = 25.4 cm	HW	2.5 10^5	isolines of U, SF observation
Taylor *et al.* (1982) [35]	90-bend, L_u=0.3 m L_d = 2.0m	D_h = 4 cm	LDA	4 10^4	U_{long} and U_{transv} and Reynolds stresses
Liou and Liu (1986) [35]	90-bend L_u=0.1 m L_d = 1.1m	D_h = 4 cm	LDA	4.2 10^4	14 half-planes normal to the curved duct walls of mean velocity and turbulence intensity
Kliafas and Holt (1987) [25]	90-bend	D_h = 10 cm	LDA	2.2 10^5 3.5 10^5	U_{long} and U_{transv} profiles at 0°, 15°, 30° and 45°
Fujita *et al.* (1989) [27]	SD, L = 4.5 m	D_h = 5 cm	HW	10^5	iso-value U_{long}, vorticity, vector-files U_{transv}
Sudo *et al.* (2001) [36]	with bend, L_u=8 m L_d = 3.2m	D_h = 8 cm	LDA	5.7 10^4	Profiles for different z/D_h
Kuan *et al.* (2007) [37]	CB, R_c = 1.5	D_h = 15 cm	LDA	10^5	vertical symmetry plane U_m, I_{turb} U_m at 1 mm from the walls

U_m : mean velocity, U velocity, I_{turb} turbulence intensity, SD : Straight Duct, R_c : turning radius, CB : curved bend, SF: secondary flows, HW: Hot Wire, PT: Pitot Tube

Table III. Experimental studies on rectangular straight ducts involving detailed flow measurements

Authors	Size	Measurement	Reynolds	Comment
Gessner and Jones (1965) [38]	L= 5.8 m, AR = 2 S = 10 x 20 cm^2	PT, HW	5 10^4, 1.5 10^5, 3 10^5	U_{transv} and Reynolds stress profiles in an octant
Melling and Whitelaw (1976) [26]	AR = 1.025 S = 4 x 4.1 cm^2	LDA, water	4.2 10^5	Contours of U_{long} and $I_{turb,}$ all 3 mean U-components and all 6 Reynolds stresses
Knight *et al.* (1985) [28]	AR=1 to 10, D_h=20 cm	ΔP	9.9 10^5	Observation of secondary flows, shear stress distributions
Fujita *et al.* (1989) [27]	L = 5 m, AR = 2, S = 10 x 5cm^2,	HW	10^5	iso-value U_{long}, vorticity, vector-files U_{transv}
S: surface of the cross-section				

3. METHODS

This study is based on experimental measurements on a large-scale duct having several singularities such as various types of bends, T-junction and reducers, completed by numerical calculations that can be used to extrapolate the experiments for cases or locations for which experimental data are not available experimentally.

3.1. Experimental facility

The experimental facility (Figure 1) is constituted mainly of large-scale rectangular ducts. This network works under aspiration by two blowers (Outlet) allowing flowrates from Q = 3000 to 5000 m^3/h for the smaller blower, and from 5000 to 12,000 m^3/h for the larger one. The facility is on three different levels,

in four different rooms, allowing for the connection of various instrumentation systems, as well as relatively easy permutations of different parts of the duct. There are three zones specifically designed for changing a given component: the "bend" zone, the "system and T-junction" zone, and the "reducer" zone. Three flow inlets are available. Through Inlet1, the air is first filtered (H13 Camfil filters, 99.95% filtration efficiency for particles with diameter 0.1 μm); it can be dehumidified down to 20% RH and heated to 20°C above the ambient temperature. Inlet2 is used without filter and dehumidification, but a 50 cm long honeycomb is installed upstream of the same heating system. Last, Inlet3 has only a metallic grid at its entrance (no honeycomb, no filter no dehumidification and no heating). Most of the duct is made up of rectangular sections measuring 40 x 60 cm^2, the reducer zone allows us to study flow through a 20 x 30 cm^2 duct section; circular sections available at different locations are of 50 cm internal diameter. The overall length is about 60 m. The duct is made of galvanized steel, except some elements which are made of Plexiglas in order to perform laser measurements as PIV.

Velocity profiles are measured by a standard Pitot tube (Pitot tube, KIMO pressure transducer) and a standard industrial hot wire anemometer (KIMO Sauermann) providing the main velocity component. The locations where the velocity profiles are performed as shown in Figure 1 (right). All the measured profiles are horizontal transverse profiles at mid-height. The number of measurement points per profile is around 30 with refinement on the walls. Each measurement point is averaged over 150 s and sampled at 1 Hz. The standard deviation on the time average is calculated on each point. Velocity profiles are obtained using a motorized displacement rail for the probe, ensuring the non-rotation of the latter by a manipulator. Each profile is reproduced at least once for at least one ventilation flowrate. About a hundred profiles have been measured, already providing a large database of results. To our knowledge, despite the simplicity of hot wire measurement, there are no experimental facilities of the same type affording so many velocity profile measurements.

Static pressure measurements are also available at many locations in the facility. Depressions in the ducts can be rather high, up to -3000 Pa in the reduced section LD11.2 downstream of experimental

measurement section of the network in order to reproduce real-scale situations. Gas tracer technique is used to calibrate the ventilation flow-rate, by measuring helium concentration using a mass spectrometer: pure helium is injected at a specific location (injection points shown on Figure 1) with a calibrated flow-rate, negligeable compared to the main duct flowrate, so that helium is considered as a trace gas and no buoyancy effect occurs; after a mixing zone, helium is considered homogeneous in the duct (this is verified experimentally), so that its concentration at one point can be used, by performing a mass balance, to determine the ventilation flow-rate. Such experiments are conducted to verify the flow transducers in the facility. They are also used during the experimental campaign, to check for potential leaks when parts of the ducts are moved from one section to another.

Repeatability on mean velocity measurements is obtained at almost all locations where measurements are performed. Many examples are given through the paper: Figure 3 for LD10, Figure 5 for L2.1 and LD2.2, Figure 7 for LD6.1, and Figure 10 for LD6.4. Self-similarity of the longitudinal component of the mean velocity is also checked in many locations and is considered to be achieved everywhere (Figure 9 bottom figure for LD6.4 and Figure 14 for LD9).

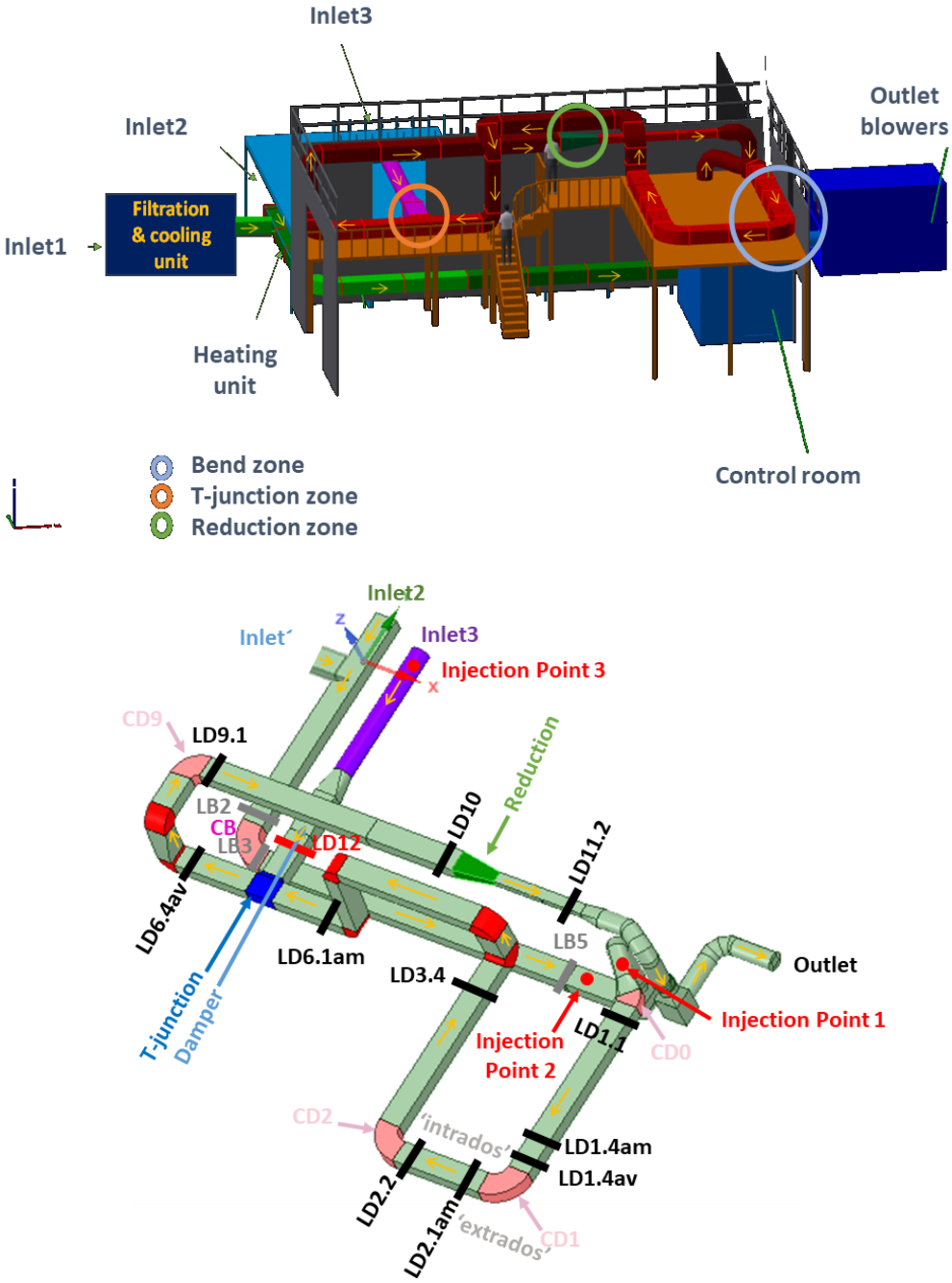

Figure 1: Overall view of the experimental facility (up) and location of the measurement zones (down) – see also Figure 8 for the T-junction zone

3.2. Numerical calculations

The numerical simulations are carried out using the ANSYS / Fluent 19.2 code. The geometry is done using SpaceClaim. The air handling unit and the fan casemate are not integrated in this geometry. The rest of ducts are simulated according to the construction plans. The mesh produced with ANSYS / Meshing is of 17 million elements, the meshes are 6 to 11 mm in length depending on the direction considered, with refinement at the walls. The calculation is carried out for isothermal conditions.

Regarding turbulence, RANS models are known to be inefficient for the characterization of secondary flows, the origin of which is known from turbulence anisotropy. This is illustrated using the standard turbulence models RANS/k-ε (RNG, Realizable) and RANS/K-ω models based on preliminary calculations of the DNS case in Zhang *et al.* (2015) [32]. This case studies flow under a friction Reynolds number Re_τ of 1200 in a square duct. With these RANS models, close agreement is obtained for the longitudinal flow, but the secondary flows are not recovered. Using RSM modeling, good results for the transverse velocity profiles are obtained (without any dedicated wall modeling, just the "enhanced wall treatment and some dedicated pressure effects" of FLUENT), as shown in Figure 2. As a result, RSM modeling is used in the calculations presented here. However, in this paper, our only concern is analysis of the average flow.

Steady state is reached between 6 and 21 s depending on the flow rates. The convergence of the residuals varies between 10^{-3} and 10^{-4} for the less efficient of the equation's highest residuals (generally from continuity equation solving), the other residuals being 10 to 100 times weaker. A Grid Independence Study was performed once on the whole facility.

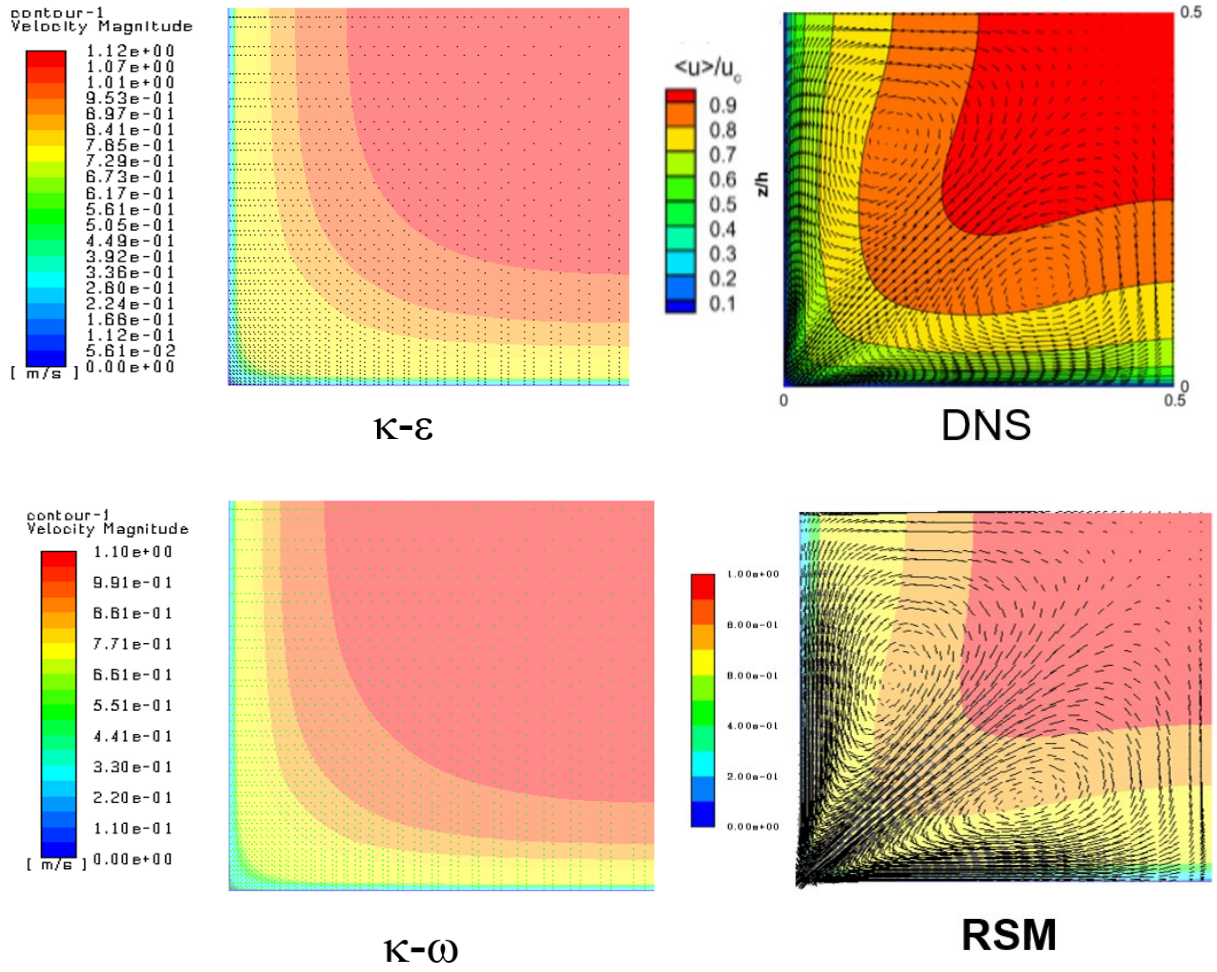

Figure 2 : Zhang *et al.* (2015) [32] DNS test case compared to two RANS modeling and the RSM

4. RESULTS AND DISCUSSION

4.1. General flow considerations

4.1.1. Establishment Length

There are many studies on the length of flow establishment, geared to specific applications. In industry (in ventilation ducts, in chimneys), for positioning instrumentation such as Pitot probes (NFX10-112, ISO 4053-1) or for injecting a tracer for specific characterization (NF X 10-141 [39]), the recommended

length for any considered flow establishment is given as between 4 and 20 hydraulic diameter D_h (the use of D_h for square channels is confirmed in Pirozzoli *et al.* 2018, [40]). In reality, the effective length considered is generally 4 D_h, mainly because industrial applications do not have long straight lengths available.

In more academic fluid mechanics, the establishment length is generally considered to be much higher, and many different relations have been developed. Anselmet *et al.* (2009) [41] provide a good review of this problem, taking into account the shape of the pipe/duct. They show that, despite the presence of secondary vortices which appear in the corners of turbulent square and rectangular ducts, the general properties of the development region of turbulence in circular pipes and square and rectangular ducts are the same and can be quantified through centerline evaluated quantities only. They also developed, based on theoretical considerations, that the laws for establishment length L_e of rectangular ducts have a scientific basis for using the hydraulic diameter D_h; they also show that these laws should necessarily be a function to the ¼ power of the Reynolds number based on the hydraulic diameter. Considering their proposed relation $L_e/ D_h = 1.3 (U_m.D_h/\nu)^{1.4}$, the parameters of the tests considered in this paper are presented in Table .

Table 4: Parameters of the different tests and flow establishment lengths

Q codification name	Q (m^3/h)	U_m (m/s)	Re (-)	L_e (m)	L_e/ D_h
Q4	3100	3.6	$1.1\ 10^5$	11.7	24
Q1	5050	5.8	$1.9\ 10^5$	13.2	27
Q2	7850	9.1	$2.9\ 10^5$	14.7	31
Q3	9272	10.7	$3.4\ 10^5$	15.4	32

Horizontal profiles of the longitudinal velocity at mid-height are obtained experimentally at location LD10 situated after almost 50 m length of ducts and 9 horizontal/vertical bends and at $L/D_h = 15.4$ downstream of the last bend, (Figure 3). The dissymmetry of this profile at this location is explained by

the fact that the flow is not, theoretically, fully developed for all the Reynolds numbers studied. This is observed experimentally as well as in the numerical simulation. However, this location is the point where the mean velocity profile is the closest to the initial flat profile. Figure 4 provides a comparison of this profile (red curve) with that obtained after a straight duct situated upstream of the first bend (yellow curve – given at a different Reynolds number than that one of Figure 3, but the flow similarity is demonstrated on many locations of the facility (see for example Figure 9, bottom figure) : the latter is the location having the longest straight lengths of duct upstream and downstream. For example, the zone $L/D_h = 18.8$ located downstream of the first bend (blue curve in Figure 4) presents a less flat velocity profile than that obtained at $L/D_h = 15.4$ downstream of the entire duct network (red curve in Figure 4). These results simply exhibit the influence of downstream singularities on the flow, which is generally well known, but not always studied in detail.

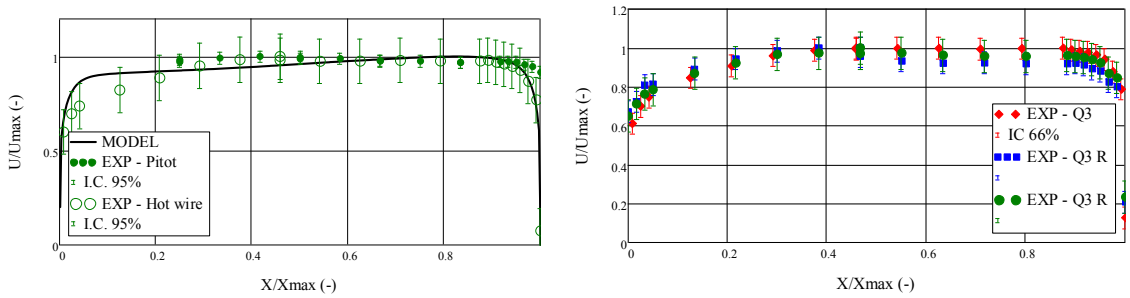

Figure 3: Horizontal profiles of the longitudinal velocity at mid-height at L/D_h = 15.4 downstream of the last bend CD9 (LD10): code-experiment comparison (left), repeatability study (right) – Re = 3.4 10^5

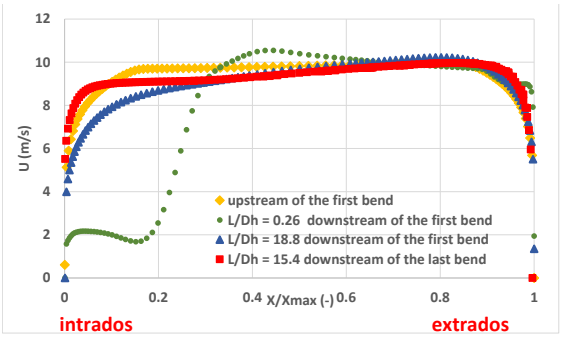

Figure 4: Numerical results - horizontal component of the mean velocity profile upstream and downstream of the first bend CB, as well as at LD10, located downstream of around 50 m of straight ducts and ten bends, at L/D_h = 15.4 downstream of the last bend CD9 – Re = 2.9 10^5

4.1.2. Bend flows

It has been seen in the previous section how a bend can influence the horizontal component of the mean velocity, even $15D_h$ to $19D_h$ downstream. The detailed evolution of the change in velocity profile downstream of a horizontal bend is given by the numerical calculations in the upper part of Figure 5. Two main parts upstream of a bend can be considered: up to a length of $3D_h$, where the flow in the inner curvature zone (the so-called intrados) changes downstream of the recirculation zone, and from $3D_h$, where the velocity profile very slowly returns to a flat profile. These numerical results downstream of a

bend are validated by the experimental data presented at two locations in the bottom part of Figure 5. It can be seen that the code-experiment agreement is very close.

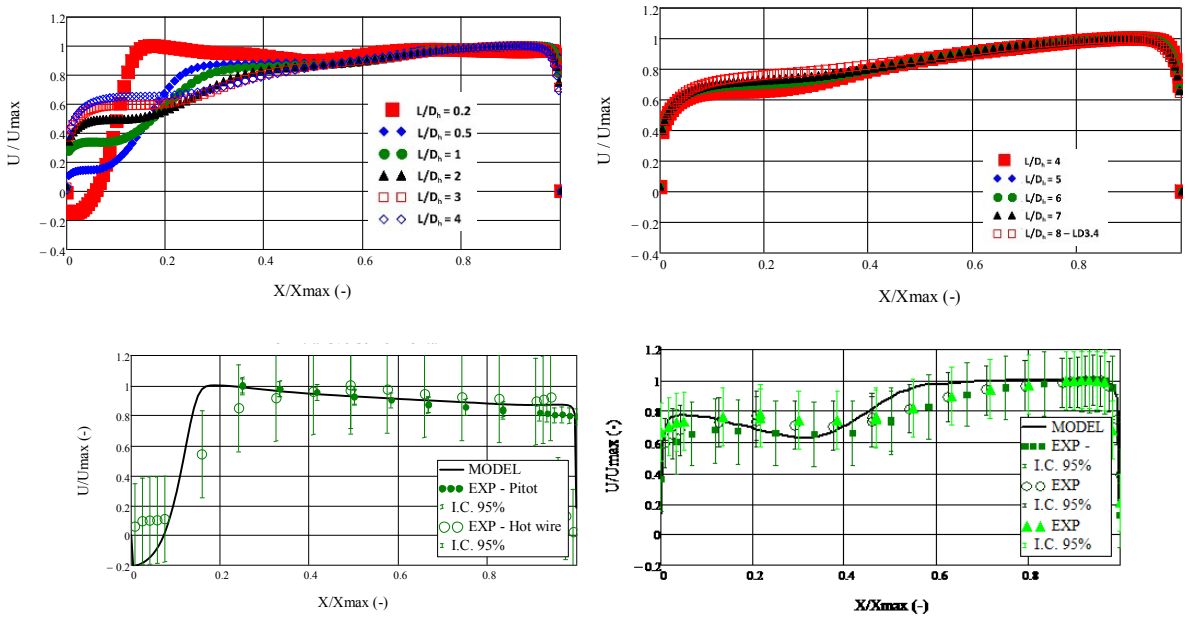

Figure 5: Horizontal component of the mean velocity profile at different distances downstream of a horizontal bend at mid-height at Re = 3.4 10^5: upper figures, simulations downstream CD2, bottom figures, code-experiment comparison downstream of CD1 at LD2.1 (L/D_h = 0.26) and LD2.2 (L/D_h = 2.5), IC 95%

Considering the flow upstream of a bend, the influence is less significant but should also be noted, as presented in Figure 6 for simulations and experiments. The maximum velocity shifts from one side of the duct (intrados) to the other (extrados). Again, the numerical results are in close agreement with the experiments.

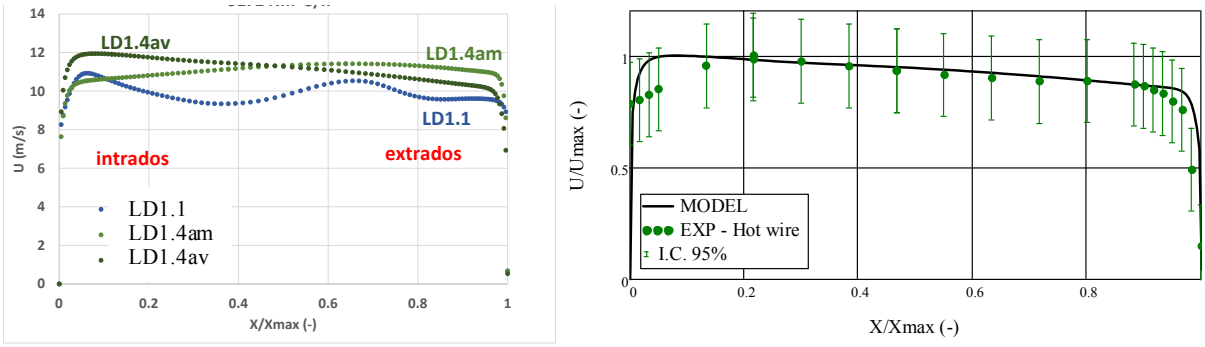

Figure 6: Horizontal component of the mean velocity profile at different distances upstream of a horizontal bend CD1 – left, simulation at LD1.4av: L/D_h = -7.8, LD1.4am = L/D_h = -0.26, LD1.1: L/D_h = -10.2), right: code-experiment comparison at L/D_h = -7.8; Re = 3.4 10^5, IC 95%

It should also be emphasized that, compared to a square duct or a circular pipe, these results on the influence of a horizontal bend are given here for the horizontal profile of the velocity at mid-height and cannot be extrapolated to the vertical profiles (no symmetry). This is confirmed by analyzing the results of a horizontal profile immediately downstream of a vertical bend (Figure 7). In both the simulation and the experiments, the velocity profile remains almost flat. The vertical profile could not be measured at that point, but it should, for symmetry and self-similarity reasons, be, very close to the bottom left one of Figure 5.

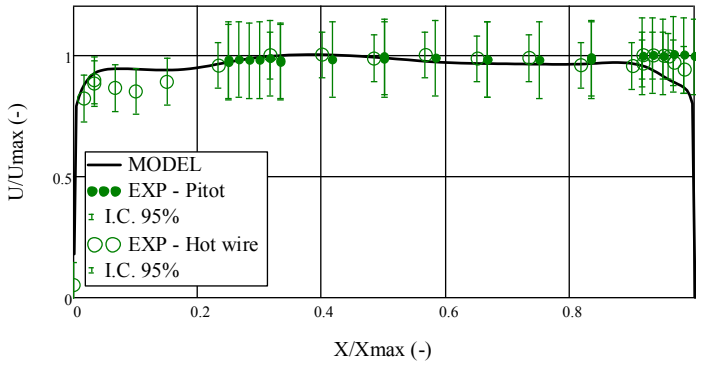

Figure 7: Horizontal component of the mean velocity profile at LD6.1: L/D_h = 0.26 downstream of a vertical bend, code-experiment comparison, Re = 3.4 10^5, IC 95%

4.1.3. T-junction flows

The flow in a horizontal T-junction (Figure 8) can also be studied in this facility, considering one main incoming branch (MInB), a perpendicular secondary incoming branch (SInB) and the outlet branch (OutB). Numerical results as well as one code-experiment comparison are presented in Figure 9. It is interesting to see some similarity for the flow in a bend and the one in a T-junction : this can be observed by comparing left graph of Figure 9 for the flow downstream of a T-junction and the left graph of Figure 5 for the flow downstream of a horizontal bend. The effect of the velocity sink due to the curvature of the duct is observed on a larger transverse zone (up to X/X_{max} = 0.2) for the bend than for the T-junction (up to X/X_{max} = 0.1): in the latter, the flow of the incoming branch avoids the larger effect observed in a bend. This observation is made for all incoming flows and is found to be self-similar in the simulations as well as in the experiments (Figure 9, bottom figure). Changing the flow in the SInB results in a change to this "typical bend flow profile" in the so-called 'intrados' (inner part of the flow curvature) between the SInB and the OutB. Such results indicate how complicated the flow in a T-junction can be, depending on the main incoming branch, the characteristics of the bend formed from the SInB and the OutB of the T-junction, and the flow repartition between the MInB and the SInB.

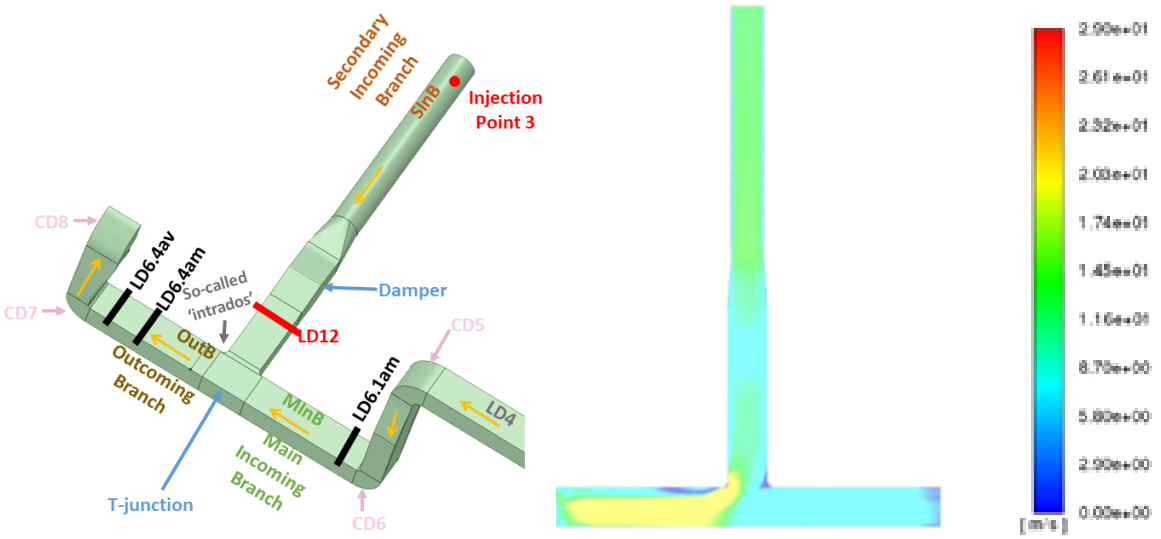

Figure 8: T-junction representation (left) and simulated field of the velocity magnitude at mid-height of the duct section (right)

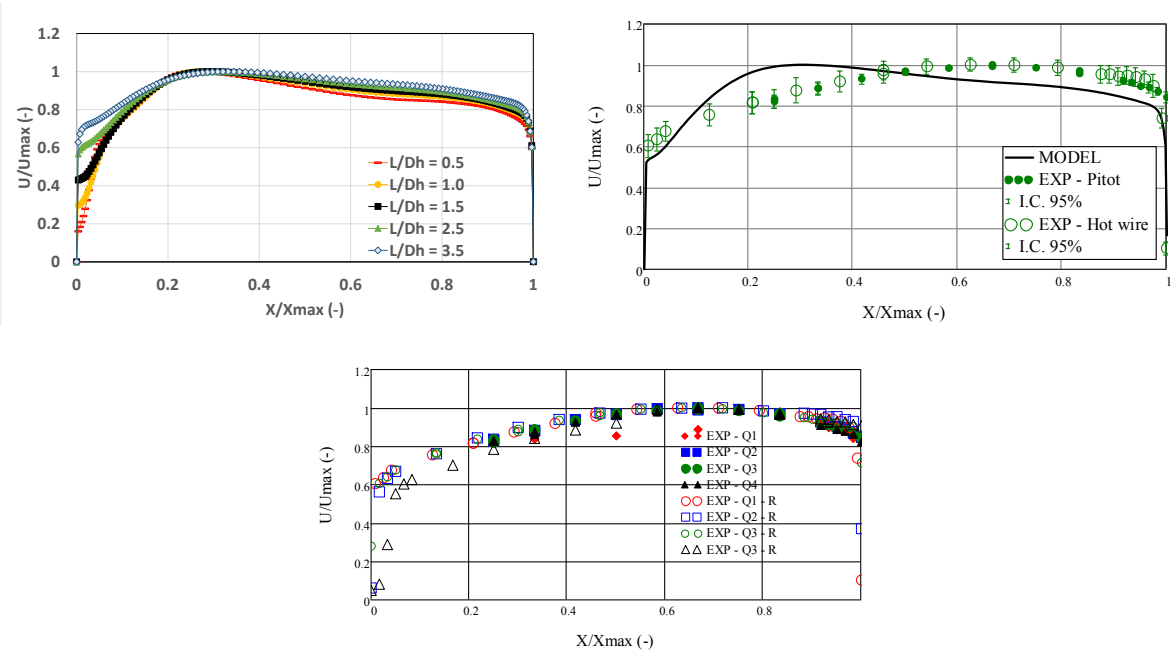

Figure 9: Horizontal component of the mean velocity profile in the OutB downstream of a horizontal T-junction with two incoming branches for Re_{MInB} = 3.0 10^5 and Re_{SInB} = 4.4 10^4 : upper figures, left :

simulations at different distances L/D_h, right code-experiment comparison at LD6.4: $L/D_h = 2$, bottom figure : experiments for the four different flowrates in the MInB at LD6.4: $L/D_h = 2$, IC 95%

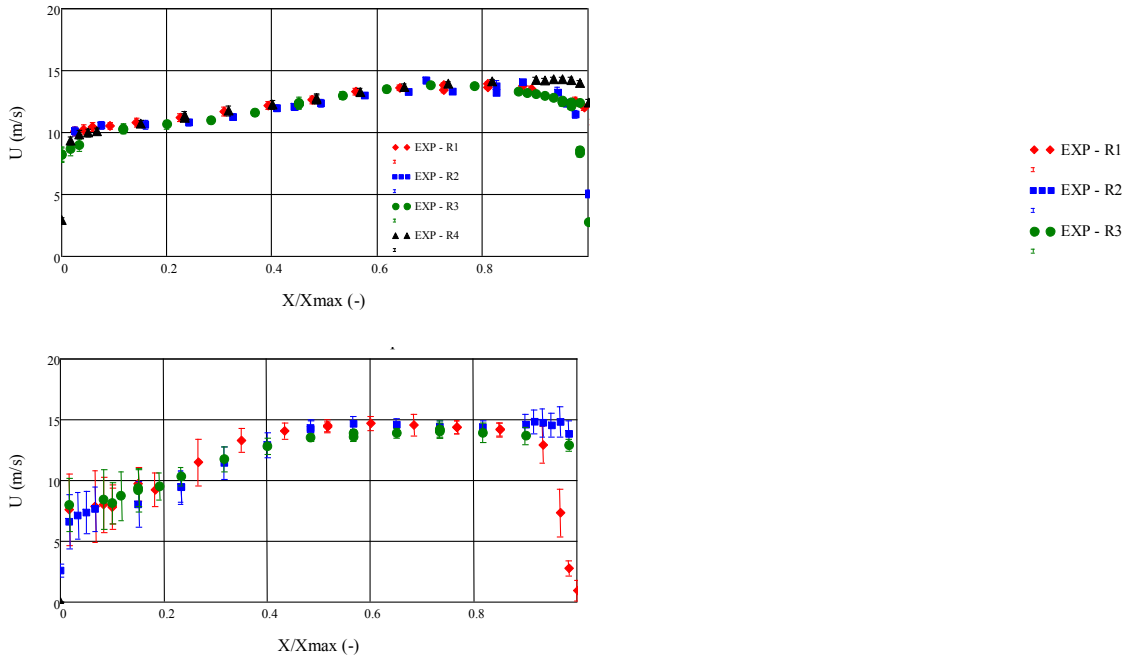

Figure 10: Horizontal component of the mean velocity profile for different flow repartition in the SInB of the T-junction; Left : $Re_{MInB} = 3.2\ 10^5$ and $Re_{SInB} = 1.8\ 10^5$, Right : $Re_{MInB} = 8.9\ 10^4$ and $Re_{SInB} = 3.4\ 10^5$ - profiles measured at LD6.4: $L/D_h = 2$

In the case of gas transfer in the main line of the T-junction, the secondary junction involves a change in the gaseous concentration. A heterogeneous concentration field can then be obtained, as illustrated in Figure 11.

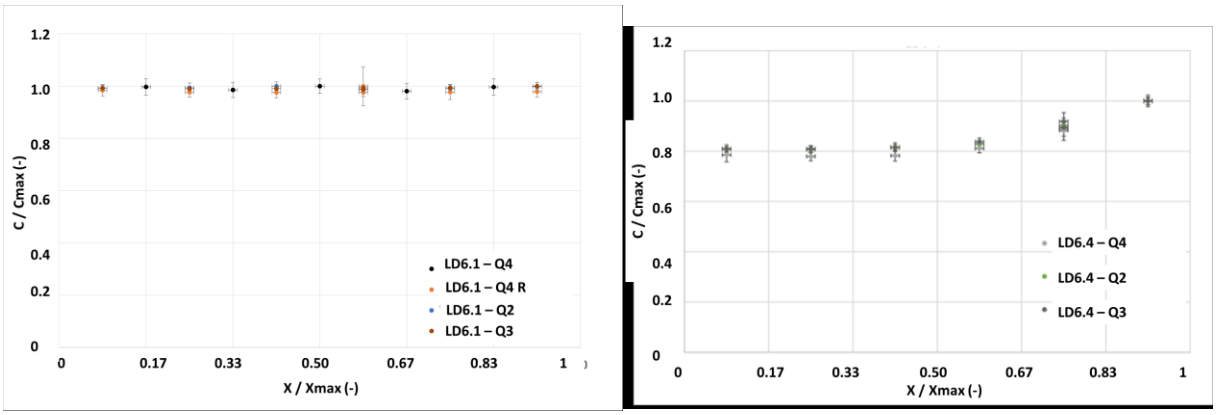

Figure 11: Effect of a secondary branch of a T-junction on gaseous concentration profile: concentration profile upstream of a T-junction at LD6.1 (L/D_h = 0.26) on the left and downstream at LD6.4 (L/D_h = 2) on the right

4.1.4. Reducer flow

The last part of this facility comprises a reducer section with the duct narrowing from 0.4 m x 0.6 m cross-section (D_h = 0.48 m) to 0.2 m x 0.3 m cross-section (D_h = 0.24 m). The reducer component is symmetrical, centered on the centers of the upstream and downstream sections, and at a 45° angle with the axis of the duct. Since the velocity profile upstream of this reducer is almost flat for a flow Reynolds number of 3.4 10^5 (Figure 3), the profile downstream of the reducer (L/D_h = 5.7) remains flat, as presented in Figure 12. Even if this result can be considered as expected, it should be emphasized that the reducer section does not result in any enhancement of the slight dissymmetry present upstream of the reducer.

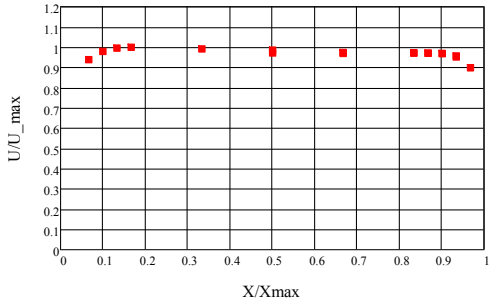

Figure 12 : Horizontal component of the mean velocity profile downstream of the reducer section (LD11.2 - $L/D_h = 5.7$)

4.2. Influence of specific industrial features on the flow

In this section, typical industrial features, such as an inner bend deflector or a ventilation damper as well as a T-junction (Figure 13) will be studied and their influence on the flow discussed.

Figure 13: Inner deflector in an industrial horizontal bend CD2 (left) and ventilation damper in an open position (right)

4.2.1. Bend deflector

In industrial ventilation networks, it is generally considered that a so-called deflector (Figure 13), inserted in a duct, is favorable to ensuring turbulence and mixing of the flow. Several bends with a deflector are

available in this facility. Experimental measurements are performed just downstream the deflector (Figure 14) and numerical calculations are given at the same location but without a specific modeling of the deflector. Experimental results show a clear effect of the deflector, and the effect is found to be self-similar. It can also be noticed that the effect of the deflector on the mean flow is no longer observed at $L/D_h = 8$ downstream (Figure 15).

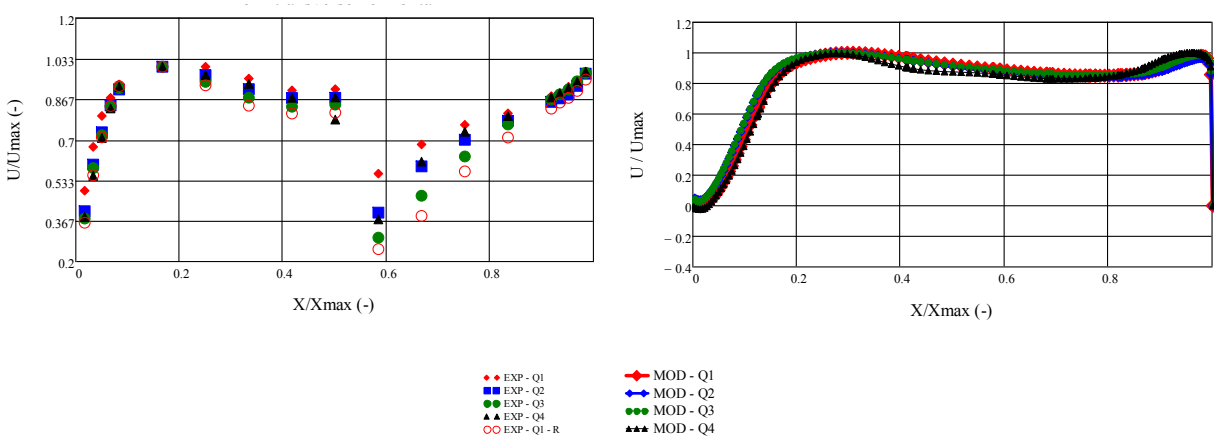

Figure 14: Horizontal component of the mean velocity profile downstream of the bend, showing the experiment with an inserted deflector in the bend on the left, and the simulations without any bend on the right – LD9 at L/D_h= 0.26

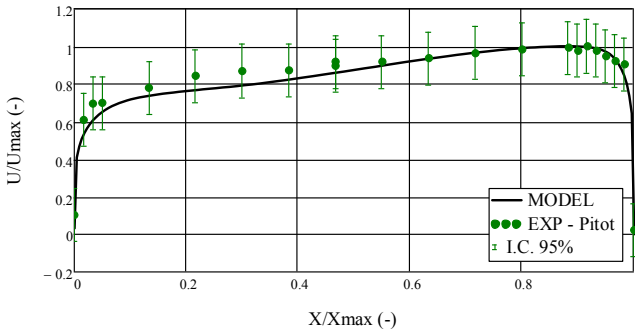

Figure 15: Horizontal component of the mean velocity profile downstream of a bend CD2 equipped with a deflector at L/D_h= 8 (LD3.4), Re = 3.4 10^5, IC 95%

4.2.2. Leak in a ventilation damper

Various classes of ventilation dampers (Figure 13) can be found in ventilation networks, classed according to intrinsic leakage level. In this facility, a Class C damper (EN 1751 standard) is tested in order to evaluate the flowrate, and as a result the velocity obtained downstream of a closed damper located upstream of the secondary branch of the T-junction. Results are presented in Figure 16, for the minimum and maximum flowrates studied here, i.e., for different depressions occurring inside the T-junction and involving aspiration through the closed damper. It can be seen that the residual leakage velocities are non-negligible and that the flow is highly fluctuating. To confirm the orientation of this leakage, helium is injected upstream of the damper and the measured helium concentration profile is almost a flat profile for the highest ventilation flowrate in the main incoming branch of the T-junction (Figure 17). These helium concentration measurements, knowing the injection flowrate of 20 l/min at the entrance of the T-junction allows also to calculate the duct ventilation flowrate in the secondary incoming branch, i.e., the leakage flowrate. This is done using the gas tracer technique described in Section 3.1. The damper leakage flowrate found from those helium concentration measurements is the used for numerical simulations. Figure 18 shows the code-experiment comparison of the velocity in the secondary incoming branch: the numerical simulations performed with a leakage flowrate through the damper are in better agreement with the experimental data than the ones considering a tight damper.

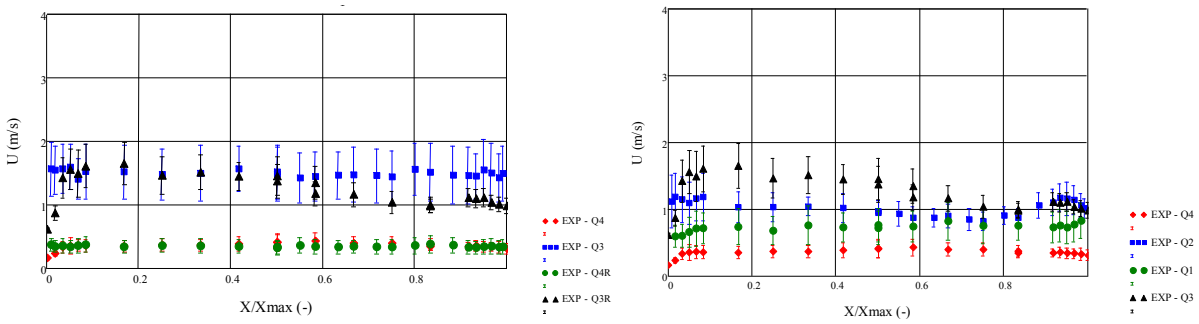

Figure 16: Horizontal component of the mean velocity profile downstream of a closed Class C damper (LD12) located on the SInB of the T-junction – On the left, repeatability study for two flow-rates, on the right, leakage flow on the SInB – Q given for the MInB (see Table), IC 66%

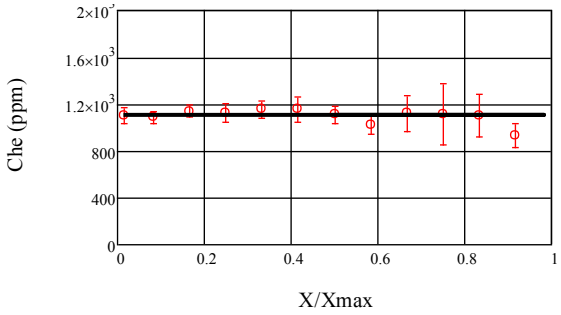

Figure 17: Helium concentration horizontal profile downstream of a closed damper having a residual leakage (Re_{SInB} = 4.4 10^4), Re_{MInB}= 3.0 10^5, IC 95%

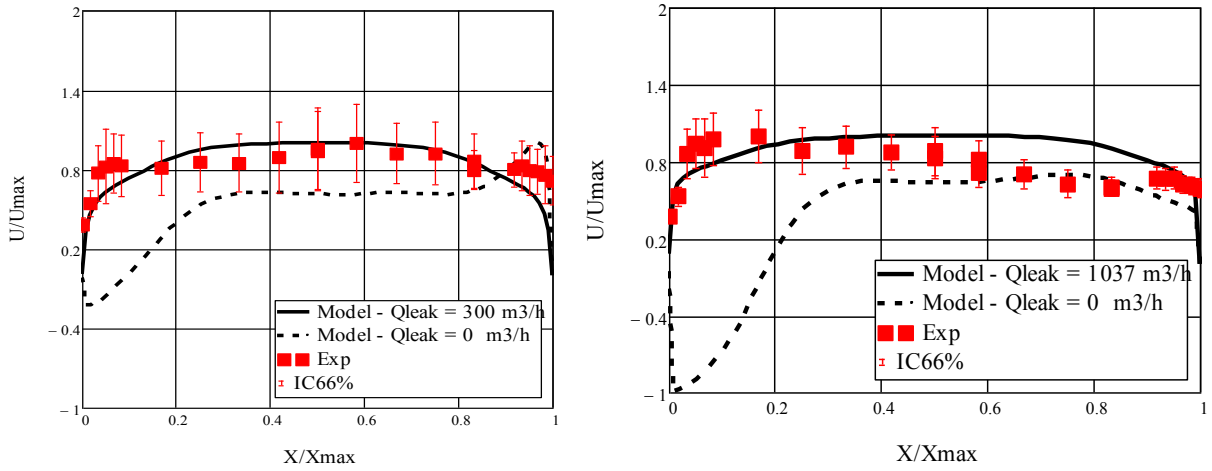

Figure 18: Code-experiment comparison of the velocity profiles in the secondary incoming branch downstream of the ventilation damper considering the presence (real damper) or absence (ideal damper) of a leakage flow in inlet3, for Q4 (left) and Q3 (right), IC66%

4.2.3. Impact of flow repartition in a T-junction

Considering that numerous simulations of the flow in this duct network have already been well validated on experimental data (part of them are presented in this paper), numerical simulations have been used to study the influence, on the velocity profile, of the flow repartition between the main incoming branch and the outcoming branch of a T-junction.

It can be observed in Figure 19 that when the flowrate in the secondary incoming branch becomes higher than the flowrate in the main incoming branch ($Q_{OutB} = 3\ Q_{MInB}$, so that $Q_{SInB} = 2Q_{MinB}$), the typical bend recirculation zone (Figure 5) is observed, as already discussed in section 4.1.3 (Figure 9). It can be concluded that the flow in a T-junction is a clear mixing of a bend flow and a straight flow and that this mixing depends on the flow distribution. A more detailed study on T-junction flows is thus needed in order to consider the shape of the T-junction as well as flow distribution in the branches.

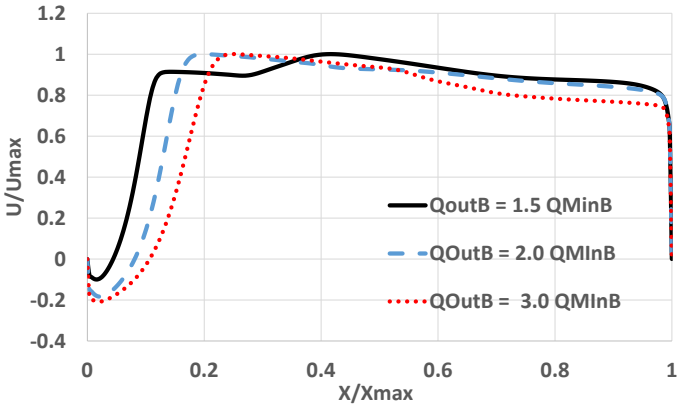

Figure 19: Horizontal component of the mean velocity profile just at the outlet of the T-junction at LD6.4 ($L/D_h = 2$), for different volume flowrates in the outlet branch of the T-junction (Q_{OutB}) as a function of the flowrate of the main inlet branch of the T-junction (Q_{MInB})

4.2.4. Impact of a ventilation damper on the flow

A ventilation damper (Figure 13) is made up of different blades to form a specific angle with the duct axis, between 90° (closed damper) and 0° (fully open damper). Its purpose is to modify the flowrate by increasing the pressure loss when this angle is changed. Despite the fact that the damper blades should generate strong turbulence and mixing, the opposite effect is observed in our experiments. A tracer gas is injected (see the injection points on Figure 1) over a 10 mm internal diameter tube centered on the duct section in a co-current manner. Concentration profiles are measured at around $10D_h$ upstream of the injection point. It can be observed that, downstream of the ventilation damper, the turbulent fluctuations are much higher than at all other measurement locations (Figure 20) and that the expected almost-flat profile is hard to obtain. This result probably depends on the type of damper, i.e., on the number of blades, shape, and the flowrates, etc. The conclusion from these first results is that attention should be paid to the flow downstream of a damper since heterogeneity can be obtained at a much higher rate than expected.

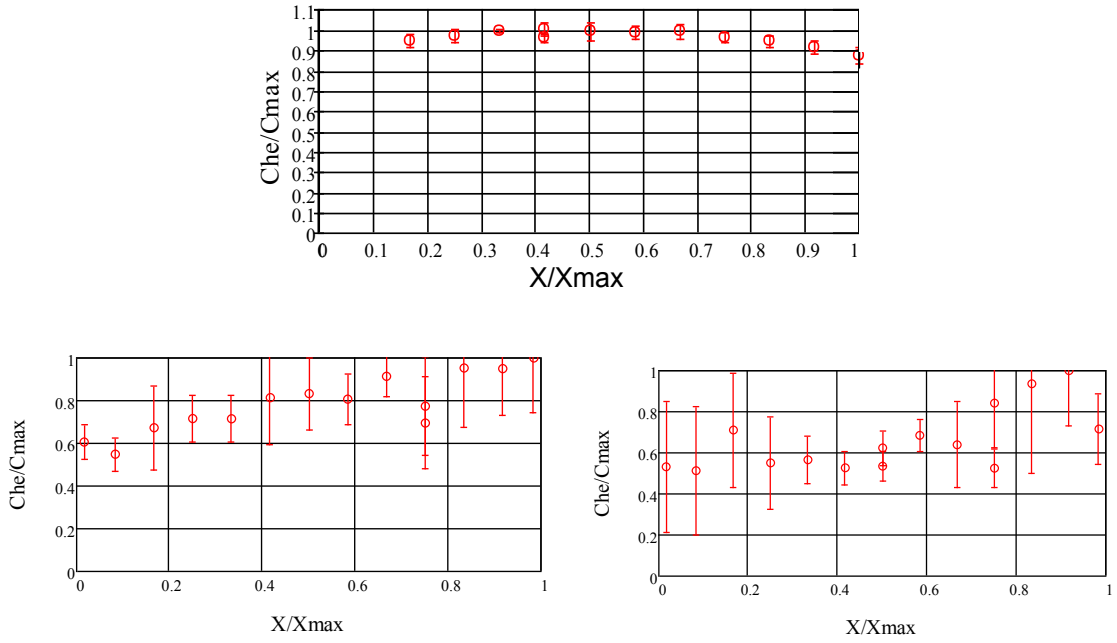

Figure 20: Effect of a damper on concentration fluctuations: top: at LD1.1, without damper upstream, bottom left: at LD12 (L/D_h= 10) with a damper half open upstream bottom right: at LD12 (L/D_h= 10) with a damper 100% open

CONCLUSION

In this paper, we have studied the characterization of the flow in various singularities of large-scale industrial ducts. The first specific feature of our study, in addition to the size of the real-scale experimental facility with 0.6 m x 0.4 m ducts measuring over 60 m in length, is that it is based on numerous experimental measurements combined with CFD simulations of the flow performed using second-order turbulence modeling (RSM), which enables anisotropy to be taken into account. In this paper, the focus is mainly on mean variables, but the metrology of this facility makes it possible to go further in the future and include PIV and high-frequency hot wire anemometry.

The simulations have first been validated for a DNS case, and numerous code-experiment comparisons are given in this paper, enabling CFD calculations with RSM turbulence modelling to be used as a prospective tool for investigating flow in zones without instrumentation.

A specific study on straight lengths shows that in such real-scale applications, flow establishment is never rigorously obtained because of both upstream and downstream singularities. However, the velocity profile at $15D_h$ is found to be almost flat in this facility. Flow downstream of a bend is also studied in this paper. Even if many other studies can be found in the literature on bend flows, this is, to our knowledge, the first research at such a scale and with such detailed measurements, on horizontal as well as vertical bends. The influence of a specific industrial component, the deflector inserted inside a bend, is shown experimentally and the velocity profiles are found to be strongly impacted by such a deflector up to $8D_h$. This result is not found in previous studies. Considering, for example, that some measurement components, such as Pitot Industrial Probes, can be installed in a shorter zone downstream of a bend with a deflector, numerous errors can be obtained in flow measurements in the presence of a deflector. A horizontal T-junction is another singularity investigated in this paper, which is rather a rare component to be studied in ventilation ducts. Flow measurements in T-junction outlets exhibit some similarity with a bend outlet; this observation could be used in future studies on engineering modeling of such flows, even if the flow distribution between the T-junction branches should be a further parameter to consider. The last singularity considered in this paper is a ventilation damper which, first, is found to have a consequent impact on the downstream flow pattern when closed (a damper is never perfectly sealed), and second, shows significant variations in concentration homogeneity downstream.

The database of experimental data acquired using this large-scale ventilation duct is important and is continuously growing. It can also be used for benchmarking activities in the field of flow simulation for mechanical ventilation. The code-experiment validations presented in this paper give some confidence in prospective use of the numerical simulations to study in more detail specific features, such as the effects of the bend curvature or the flow repartition in a T-junction. The results can also serve as the basis for

flow validation before studying many other physical phenomena which depend on the flow, such as gas dispersion and aerosol deposition in ventilation ducts. This database could be enlarged with turbulence variables using transparent singularities coupled with PIV measurements.

NOMENCLATURE

C : concentration

C_{he} : helium concentration

C_{max} : maximum helium concentration of the considered profile

D_h : hydraulic diameter

FT04 : flowrate at the reducer zone

HW : hot-wire

IC : interval of confidence

L_d : downstream length

LDA : laser doppler anemometry

L_e : flow establishment length

L_u : upstream length

L_o : downstream length

L/D_h : non-dimensional distance in the duct, having its origin at the outlet of the singularity located just upstream/downstream of the considered length

MInB : indices for Main Incoming Branch of a T-junction

OutB : indices for outcoming Branch of a T-junction

PIV : particle image velocimetry

PT : pitot tube

PT04 : pressure at the reducer zone

Q : volume flowrate

Q_{iR} : repeatability study at Q_i

r : radial direction

R_c : curvature radius

Re : Reynolds number based on the duct hydraulic diameter and the duct mean velocity

Re_τ : Reynolds number based on the duct hydraulic diameter and the friction velocity

RH : relative humidity

SP : static pressure measurement

SInB : indices for Secondary Incoming Branch of a T-junction

U_m : mean velocity

U_{max} : maximum velocity of the considered profile

U_{long} : longitudinal velocity component

U_{transv} : transverse velocity component

X : horizontal length in of the duct section

X_{max} : maximal length of considered profile (i.e. duct section)

z : longitudinal direction, where z = 0 is the duct or the singularity entrance, depending on context

ν : kinematic viscosity

Acknowledgements

The authors would like to thank the R. Rossignol and D. Hare for their contribution to some of the T-junction characterization data.

REFERENCES

[1] DIN EN 12599-Ventilation for buildings-Test procedures and measurement methods to hand over air conditioning and ventilation systems

[2] Dinardo G., L. Fabbiano, G.o Vacca, How to directly measure the mean flow velocity in square cross-section pipes, Flow Measurement and Instrumentation, Vol. 49, pp. 1-7, 2016

[3] Sippola M. R., Nazaroff W. W., Experiments Measuring Particle Deposition from Fully Developed Turbulent Flow in Ventilation Ducts, Aerosol Science and Technology, 38:9, 914-925, 2004

[4] Wu J., Zhao B., Effect of ventilation duct as a particle filter, Building and Environment vol. 42, pp. 2523–252, 2007

[5] Ben Othmane M., Havet M, Gehin E., Solliec C., Arroyo G., Predicting cleaning time of ventilation duct systems in the food industry J. Food Eng. 105 400–7, 2011

[6] Jiang H., L. Lu, K. Sun, Experimental study and numerical investigation of particle penetration and deposition in 90° bent ventilation ducts, Building and Environment, Vol. 46, pp. 2195-2202, 2011

[7] Lu, H., Wang, Y. Particle deposition in ventilation ducts: A review. Build. Simul. Vol. 12, pp. 723–734, 2019

[8] Costa D., Malet J. Géhin E., Dry aerosol particle deposition on indoor surfaces: Review of direct measurement techniques, Aerosol Science and Technology, Vol. 56, pp. 261-280, 2022

[9] Lain and Sommerfeld, Stochastic modelling for capturing the behaviour of irregular-shaped non-spherical particles in confined turbulent flows, Powder Technology, Volume 332, Pages 253-264, 2018

[10] Afram A., Janabi-Sharif F., Review of modeling methods for HVAC systems, Applied Thermal Engineering, Volume 67, Issues 1–2, pp. 507-519, 2014

[11] Chojnacki E. W. Plumecocq L. Audouin, An expert system based on a Bayesian network for fire safety analysis in nuclear area, Fire Safety Journal, Volume 105, pp. 28-40, 2019

[12] Hinze, J. O. Experimental investigation of secondary currents in the turbulent flow through a straight conduit. Appl. Sci. Res. 28, 453–465, 1973

[13] Rokni, M., Olsson, C., Sundén, B., Numerical and Experimental Investigation of Turbulent Flow in a Rectangular Duct, Int. J. Numer. Methods Fluids, 28(2), pp. 225–242, 1998

[14] Geropp D., Odenthal H.-J., Flow rate measurements in turbulent pipe flows with minimal loss of pressure using a defect-law, Flow Measurement and Instrumentation, vol. 12, pp. 1-7, 2002

[15] Sudo K., M. Sumida, H. Hibara, Experimental investigation on turbulent flow in a circular-sectioned 90-degree bend, Experiments in Fluids 25, pp. 42-49, 1998

[16] Kalpakli A., Orlu R., Turbulent pipe flow downstream a 90° pipe bend with and without superimposed swirl, International Journal of Heat and Fluid Flow, Volume 41, pp. 103-111, 2013

[17] Azzola J., Humphrey J. A. C., Iacovides H., Launder B. E., Developing Turbulent Flow in a U-Bend of Circular Cross-Section: Measurement and Computation, 1986

[18] Sudo K., Sumida M., Hibara H., Experimental investigation on turbulent flow through, a circular-sectioned 180° bend, Experiments in Fluids, 28, pp. 51-57, 2000

[19] Caré I., Bonthoux F., Fontaine J.R., Measurement of air flow in duct by velocity measurements, 16th International Congress of Metrology, Volume 77, 2014

[20] Sleiti A., Salehi M., Stephen Detailed velocity profiles in close-coupled elbows—Measurements and computational fluid dynamics predictions (RP-1682), Science and Technology for the Built Environment, 23:8, pp. 1212-1223, 2017

[21] Enayet M.M., Gibson M.M., Yianneskis M., Measurements of turbulent developing flow in a moderately curved square duct, International Journal of Heat and Fluid Flow, Volume 3, Issue 4, pp. 221-224, 1982

[22] Demuren A. O., W. Rodi, Calculation of turbulence-driven secondary motion in non-circular ducts, Journal of Fluid Mechanics, vol. 140, pp. 189-222, 1984

[23] Launder B. E., W. M. Ying, Secondary flows in ducts of square cross-section, Journal of Fluid Mechanics, vol. 54, n° 12, pp. 289-295, 1972

[24] Gessner F. B., Jones J. B., On some aspects of fully developed turbulent flow in rectangular channels, J. Fluid Mech. Vol. 33, pp. 689-713, 1965

[25] Kliafas Y., M. Holt, LDV measurements of a turbulent air-solid two-phase flow in a 90 ° bend, Experiments in Fluids, Vol. 5, pp. 73-85, 1987

[26] Melling, A., Whitelaw, J. H., Turbulent Flow in a Rectangular Duct, Journal Fluid Mechanics, Vol. 78, Part 2, pp. 289-315, 1976

[27] Fujita H., H. Yokosawa et M. Hirota, Secondary flow of the second kind in rectangular ducts with one rough wall, Experimental Thermal and Fluid Science, vol. 2, n° 11, pp. 72-80, 1989

[28] Knight D.W, H. S. Patel, Boundary shear in smooth rectangular ducts, Journal of Hydraulic Engineering, vol. 111, n° 11, pp. 29-47, 1985

[29] Maeda N., M. Hirota, H. Fujita, Turbulent flow in a rectangular duct with a smooth-to-rough step change in surface roughness, Energy, Vol. 30, Issues 2–4, pp.129-148, 2005

[30] Huser A., S. Biringen, Direct numerical simulation of turbulent flow in a square duct, J. Fluid Mech., vol. 257, pp. 65-95, 1993

[31] Gavrilakis S., Numerical simulation of low-Reynolds-number turbulent flow through a straight square duct, J. Fluid Mech., vol. 244, pp. 101-129, 1992

[32] Zhang H., F. X. Trias, A. Gorobets, Direct numerical simulation of a fully developed turbulent square duct flow up to Re_τ= 1200, International Journal of Heat and Fluid Flow, vol. 54, pp. 258-267, 2015

[33] Brundrett E. and Baines D. (1964), The production and diffusion of vorticity in duct flow, Journal of Fluid Mechanics, vol. 19, n°13, pp. 375-394, 1964

[34] Taylor A. M. K. P., Whitelaw J. H., Yianneskis M., Curved Ducts with Strong Secondary Motion: Velocity Measurements of Developing Laminar and Turbulent Flow, Journal of fluid Engineering, Volume 104, Issue 3, 1982

[35] Liou T.M., Liu C.S, Turbulence measurements in a 90°square duct using laser- Doppler velocimetry, Journal of the Chinese Institute of Engineers, Vol. 9:1, pp. 19-25, 1986

[36] Sudo K., M. Sumida, H. Hibara, Experimental investigation on turbulent flow in a square-sectioned 90-degree bend, Experiments in Fluids 30, 246-252, 2001

[37] Kuan B., Yang W., Schwarz M.P., Dilute gas–solid two-phase flows in a curved 90◦ duct bend: CFD simulation with experimental validation, Chemical Engineering Science 62, pp. 2068 – 2088, 2007

[38] Gessner F. B., J. K. Po, A. F. Emery, Measurements of developing turbulent flow in a square duct, Turbulent Shear Flows I. Springer, pp. 119-136, 1979

[39] AFNOR standard, Measurement of gas flow in conduits - Tracer methods, NF X 10-141, ICS 17.120.10, 1982

[40] Pirozzoli S., Modesti D., Orlandi P., Grasso F., Turbulence and secondary motions in square duct flow, J. Fluid Mech., vol. 840, pp. 631–655, 2018

[41] Anselmet F., F. Ternat, M. Amielh, O. Boiron, P. Boyer, L. Pietri, Axial development of the mean flow in the entrance region of turbulent pipe and duct flows, Comptes Rendus Mécanique, Volume 337, Issue 8, pp. 573-584, 2009